International Journal of Nanoelectronics and Materials
IJNeaM
ISSN 198-5761 | E-ISSN 2232-1535

Arthropods-mediated Green Synthesis of Zinc Oxide Nanoparticles using Cellar Spider Extract: A Biocompatible Remediation for Environmental Approach

M. Isa[a], M. N. A. Uda[a,b,c,*], M. A. R. Irfan[b], Uda Hashim[a], Subash C. B. Gopinath[a,d], Hafiza Shukor[d] ,M. N. Afnan Uda[e] , MRM Huzaifah[f] Maimunah Mohd Ali[g] N. H. Ibrahim[d], Muaz Mohd Zaini Makhtar[i] , Qi Hwa Ng[d], M. K. R. Hashim[b] , Z. A. Arsat[b], N. A. Parmin[a], Liyana Ahmad Sofri[h], Mahfuz Affif Mohd Ruslan[d] and Tijjani Adam[a]

[a]*Institute of Nano Electronic Engineering, Universiti Malaysia Perlis, 01000 Kangar, Perlis, Malaysia.*
[b]*Faculty of Mechanical Engineering & Technology, Universiti Malaysia Perlis, Kampus Tetap Pauh Putra, 02600 Arau, Perlis, Malaysia.*
[c]*Centre of Excellence for Biomass Utilization, Universiti Malaysia Perlis, Arau 02600, Perlis, Malaysia.*
[d]*Faculty of Chemical Engineering & Technology, Universiti Malaysia Perlis, 02600 Arau, Perlis, Malaysia.*
[e]*Faculty of Engineering, Universiti Malaysia Sabah, 88400 Kota Kinabalu, Sabah, Malaysia*
[f]*Department of Crop Science, Faculty of Agricultural and Forestry Sciences, Universiti Putra Malaysia Bintulu Campus, 97000 Bintulu, Sarawak, Malaysia.*
[g]*Department of Food Sciences, Faculty of Science and Technology, Universiti Kebangsaan Malaysia, 43600, Selangor, Malaysia.*
[h]*Faculty of Civil Engineering & Technology, Universiti Malaysia Perlis, 02600 Arau, Perlis, Malaysia.*
[i]*School of Industrial Technology Division, Universiti Sains Malaysia, 11800, Penang, Malaysia.*
**Corresponding author. Tel.: +604 988 5035; fax: +604 988 5034; e-mail: nuraiman@unimap.edu.my*

ABSTRACT

This study presents an eco-friendly approach to synthesizing zinc oxide nanoparticles (ZnO NPs) using extracts from cellar spiders, addressing environmental and health concerns associated with conventional methods. The spider extract efficiently reduced zinc acetate dihydrate, and the synthesized ZnO NPs underwent comprehensive quantitative characterization, including size, shape, morphology, surface chemistry, thermal stability, and optical properties using Fourier-transform infrared spectroscopy (FTIR), X-ray diffraction (XRD), zeta potential measurements, thermogravimetric analysis (TGA), and UV-vis spectroscopy. The nanoparticles exhibited intended characteristics, and their adsorption capability for methylene blue (MB) was quantitatively assessed using the Freundlich isotherm model and pseudo-second-order kinetic model, providing numerical insights into MB removal efficiency. The study demonstrates the potential of these green-synthesized ZnO NPs for applications in environmental remediation, wastewater treatment, and antibacterial therapies, contributing to both sustainable nanomaterial development and quantitative understanding of their functional properties.

Keywords: *Arthropods, Cellar Spider, Morphological Study, Synthesis Nanoparticles, Zinc Oxide*

1. INTRODUCTION

Nanotechnology enhances both farm yield and quality where this innovative approach not only boosts productivity but also sets new benchmarks for effectiveness in comparison to conventional techniques [1–5]. Nanoparticles of precise shapes and sizes have been synthesized using physical, chemical, and biological processes [6–9]. Researchers are developing simple, effective, and trustworthy green nanomaterial fabrication methods. Green synthesis produces nanoparticles using environmentally friendly methods. Its cost-effectiveness and environmental friendliness make it scalable and less harmful than chemically generated nanoparticles [9]-[10]. Green synthesis uses plant extracts and bacteria, making it cost-effective, non-toxic, and ecologically beneficial [12]. To prevent harmful consequences, green synthesis must be dependable, sustainable, and ecologically beneficial. Green nanoparticle manufacturing reduces harmful chemical waste and promotes sustainability [13].

Recently there have been a lot of biological reagents used for capping for synthesis nanoparticles however less information using arthropods. Like other arthropods such as insects and arachnids are promising green synthesis candidates. Arthropods provide bioactive chemicals sustainably due to their abundance and simplicity of large-scale production. Their ability to produce large amounts of bioactive chemicals quickly boosts their appeal as a source. Green synthesis uses arthropods, a broad collection of creatures that produce bioactive substances. Arthropod-based green synthesis methods are cost-effective and commercially scalable. These processes employ moderate conditions instead than harsh chemicals or solvents, making them ecologically friendly. Biocompatible arthropod-derived bioactive chemicals reduce the risk of adverse responses in live creatures [14]. For instance, to underscore the advantages of cellar spiders, the silk fibers crafted by orb-weaving spiders stand out as some of the most formidable, pliable, and durable biomaterials acknowledged by the scientific community.

With that, this study was carried out to explore the potential of cellar spider for synthesis of Zinc oxide nanoparticles (ZnO NPs). These nanoparticles have excellent optical, electrical, and catalytic capabilities, making them useful in electronics, optoelectronics, catalysis, sensing, and biomedicine [15]. ZnO NPs' broad band gap and vast surface area make them useful. Green synthesis of ZnO NPs is attractive due to its environmental friendliness and possibility for large-scale manufacturing without harmful chemicals [16]. Green nanoparticle production uses natural resources, plant extracts, or biological agents as reducing and stabilizing agents . Zinc oxide nanoparticles are safe cleansers and antimicrobials. Antibacterial, antifungal, and antiviral activities make them useful in cell line investigations, dye degradation, and antibacterial research. Zinc oxide nanoparticles damage membrane structures and kill bacteria due to their permeability. ZnO NPs' nanosized and high surface area-to-volume ratio make them effective[17]. ZnO nanostructures have been used as antibacterial agents in healthcare, cosmetics, food storage, textile coating, and environmental applications, but their toxicity and biological activity need further study [18]. Zero-dimensional ZnO NPs range from 1 to 100 nm [19].

Bioremediation removes contaminants using bacteria, fungus, or plants. Due of its large surface area, reactivity, and antibacterial activity, ZnO NPs have been explored for bioremediation. ZnO NPs catalyst pollutant breakdown with certain microorganisms or enzymes. They also form stable complexes with metal ions to remove heavy metals from polluted locations by limiting their mobility and toxicity. However, nanoparticles may harm the environment and humans, requiring careful study and regulation to assure their safe and effective use [20–24].

2. MATERIAL AND METHODS

2.1 Extraction of Cellar Spider and Its Preparation

A total of one hundred cellar spiders were rounded up and put alive inside of bottles. In order to get the extract of the cellar spider, one hundred milligrammes of the cellar spider were combined with ten millilitres of 0.1M sodium hydroxide (NaOH) in a beaker. Following the distillation of the mixture at 90 °C for one hour, it was allowed to cool before being centrifuged at 5000 rpm for twenty minutes [25]. During the process of separating the filtrate from the supernatant, which contained the extract we were looking for, we collected the supernatant. The procedure was carried out three more times so that a total amount of cellar spider extract containing 500 millilitres could be obtained. After keeping the extract at room temperature and covering it with aluminium foil for the night, it was then placed in the dark and maintained there for further synthesis in a beaker. As depicted in Fig. 1 the extraction of cellar spider and its preparation. The alteration in the hue of the reaction mixture, consisting of zinc acetate dehydrate solution and extract derived from cellar spiders, facilitated the formation of ZnO NPs, commonly referred to as zinc oxide nanoparticles. The reduction process required for obtaining ZnO NPs was verified through the transition in color, shifting from a pale yellow shade to white within the reaction mixture containing cellar spider extract and zinc acetate dehydrate. Initially, a transparent solution of zinc acetate dehydrate is subjected to treatment with subterranean spider extract, resulting in the emergence of a color resembling light yellow. Subsequently, the color shifts to white, ultimately yielding a white powder after the drying process, representing the formation of ZnO NPs [32].

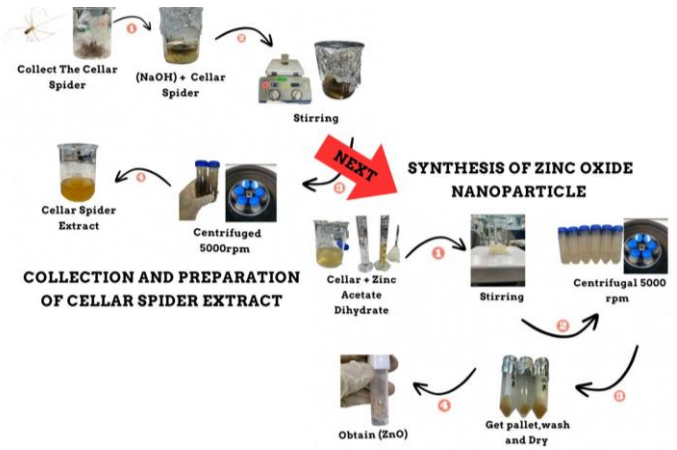

Figure 1. ZnO NPs synthesis via color changes in reaction mixtures: (a) 100mg Cellar Spider, (b) Cellar Spider + NaOH, (c) Cellar Spider extract, (d) pale yellow to white with zinc acetate dehydrate, (e) centrifugation preparation, (f) ZnO NPs pellet after 6000 rpm, (g) white ZnO NPs powder after 1-night drying.

2.2 Synthesis of Zinc Oxide Nanoparticle

The cellar spider extract is used to reduce zinc acetate dihydrate (Zn $(CH_3CO_2)_2{\cdot}2H_2O$) to stable ZnO NPs. Dissolving 46 g of Zinc acetate powder in 100 ml of distilled water yielded a 2.5M solution. 15 ml of the cellar spider extract from its preparation was put to a beaker with 30 ml of Zinc acetate solution. Aluminium foil shielded the beaker from light. After 2 hours of stirring, the cellar spider extract and zinc metal ions from Zinc acetate reacted, changing the solution's colour from light yellow to white. The mixture was transferred to an Eppendorf tube and centrifuged at 5000 rpm for 15 minutes. The supernatant was discarded, leaving the ZnO NP pellet in the tube. The particle was carefully rinsed with distilled water and centrifuged again at 5000 rpm for 15 minutes, discarding the supernatant. This washing procedure was repeated with 10% ethanol to eliminate contaminants and collect pure ZnO NPs pellets. After washing and centrifugation, the particle was dried overnight at 60 °C [26]. Pulverised dry material was kept in an airtight container at room temperature for future investigation.

To underscore the advantages of cellar spiders, this study aims to achieve the following objectives: conduct a quantitative analysis of the ZnO NPs' size, shape, and morphology through techniques including X-ray diffraction (XRD), zeta potential measurements, and thermogravimetric analysis (TGA); investigate the surface chemistry of the nanoparticles by quantitatively assessing

functional groups via Fourier-transform infrared spectroscopy (FTIR); evaluate the thermal stability of the ZnO NPs through detailed TGA; quantitatively analyze their optical properties using UV-vis spectroscopy; and assess the adsorption capability for methylene blue (MB) through quantitative models such as the Freundlich isotherm and pseudo-second-order kinetic model.

2.3 The Zinc Oxide Nanoparticle Characterization

2.3.1 Fourier-Transform Infrared Spectroscopy (FTIR)

FTIR analysis, a homogeneous mixture of 1g zinc oxide nanoparticle powder and 1g potassium bromide (KBr) powder is prepared. This mixture is pressed into a pellet using a pellet press or by hand. The resulting pellet is then placed on the sample stage of the FTIR instrument. The instrument collects a spectrum by measuring the absorption of infrared radiation at different frequencies in the mid-infrared range. The obtained spectrum is analyzed to identify absorption peaks corresponding to chemical functional groups. The spectrum is collected in the mid-infrared range, which spans from 4000 to 400 cm^{-1}. To determine the composition chemical availability in the sample, the spectrum is compared with reference spectra of pure ZnO nanoparticles and other forms of ZnO. This comparison allows for the identification of chemical availability present in the sample [27].

2.3.2 X-ray Diffraction Analysis (XRD)

Powder containing 5 mg of ZnO NPs was suspended in 50 µl of distilled water. After a period of absorption, 30 µl of solution was deposited on a spotless wafer and allowed to dry. Next, the wafer is observed at a working distance of 8 mm. Using a DMAX-2500 instrument from Rigaku, Japan, X-ray diffraction (XRD) was used to determine the crystalline structure of the synthesised zinc oxide nanoparticles. A nickel filter and a Cu Ka (1.54059 A) radiation source were utilised to prepare the operational configuration. The diffraction angle range for the XRD analysis was 10° to 90°, and the scanning rate was 0.5/s. The operational system was configured with a filament current and voltage of 40 mA and 45 kV, respectively [28].

2.3.3 Zeta Potential Characterization

Using the zeta potential method, the surface charge of nanoparticles in colloidal solutions is measured. In order to determine the surface charge of ZnO NPs, a sample of 10 mg is prepared in 20 ml of distilled water. The zeta potential and zeta size distribution of the nanoparticles are measured using a Zeta Potential Analyzer, such as the Malvern zeta-sizer nano series. Negative zeta potential values indicate a negatively charged surface, while positive values indicate a positively charged surface. The zeta potential values also reflect the nanoparticles' stability in solution, with a greater absolute value indicating greater stability [29]

2.3.4 Thermogravimetric Analysis (TGA)

Weigh 10 mg of the ZnO nanoparticles and place them in a TGA sample pan. Heat the sample pan at a constant rate while measuring the weight of the sample as a function of temperature. The temperature range used for TGA is typically 25°C to 700°C. The upper temperature used for TGA is normally 1000°C. The heat-up rate capability of TGA can vary from 0.1°C to 200°C/min. Observe the weight loss of the sample as a function of temperature to determine the thermal stability of the nanoparticles [30].

2.3.5 UV-Visible Spectroscopy

The UV-vis energy range for the electromagnetic spectrum spans 1.5 to 6.2 eV, which corresponds to the wavelength range of 900 to 200 nm. In order to prepare the mixture for UV-Visible spectroscopy analysis, 3 mg of ZnO NPs material was dissolved in 3 ml of sterile distilled water. UV-Vis spectroscopy involves passing UV-Vis light through a sample and measuring the sample's light transmission. Absorption can be calculated from transmittance (T) using the formula A=-log (T) [28].

2.3.6 Water Absorption Activity

In the kinetic study, a 20 mg sample of ZnO NPs was added to a 20 mL bottle containing a 20-ppm concentration of methylene blue (MB) solution. The mixture was shaken at room temperature and 150 rpm for various time intervals (3 min, 5 min, 10 min, 20 min, 40 min, 60 min, 90 min, and 120 min), and the solution's concentration was measured using a UV-Vis spectrophotometer within the range of 650-680 nm. For the isotherm study, a 20 mg sample of ZnO NPs was added to a 20 mL bottle containing different concentrations of methylene blue (MB) solution ranging from 10 ppm to 50 ppm, shown in Fig. 2.

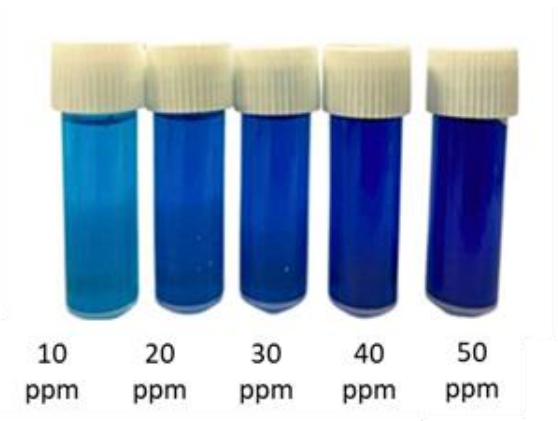

Figure 2. Concentrations of methylene blue (MB) solution ranging from 10 ppm to 50 ppm.

The mixture was shaken for 1 hour at room temperature and 150 rpm. The concentration of the supernatant was measured using a UV-Vis spectrophotometer at approximately 664 nm, the commonly used wavelength for MB analysis. Investigate the adsorption behavior of ZnO NPs towards methylene blue by examining the kinetics of adsorption at different time intervals and the isotherms at various MB concentrations. The UV-Vis spectrophotometer

measurements provided valuable data for understanding the adsorption process and the interactions between ZnO NPs and methylene blue molecules [31].

3. RESULTS AND DISCUSSION

3.1 Characterization of The Synthesized ZnO Nanoparticles

3.1.1 Fourier-Transform Infrared Spectroscopy (FTIR)

Figure 3 depicts the spectrum showing multiple peaks, reflecting the complex nature of cellar spider. The FTIR spectra of raw Cellar spider (red line) and ZnO NPs (blue line) are displayed. The peak at 3200-3500 cm-1 signifies the presence of surface hydroxyl groups (-OH) due to adsorbed water or hydroxyl groups on the nanoparticle surface [33]. The Cellar spider extract solution exhibits a peak at 3277.00 cm-1, indicating the presence of hydroxyl groups. Peaks in the range of 2800-3000 cm-1 typically arise from C-H stretching vibrations, possibly originating from organic compounds adsorbed on the nanoparticle surface or solvent residues [34]. Both Cellar spider raw and ZnO NPs show peaks at 2922 cm-1 and 2924 cm-1 (ZnO NPs), indicating single bonds. The peak at 1640-1650 cm-1 suggests the presence of water molecules adsorbed on the nanoparticle surface [35]. The peak at 1000-1350 cm-1 corresponds to the stretching vibration of the carbon-nitrogen (C-N) bond, found in amines, amides, or nitriles [36]. Raw Cellar spider displays peaks at 1069 cm-1 and 1235 cm-1, while ZnO NPs exhibit peaks at 1025 cm-1 and 1342 cm-1, indicating the presence of carbon-nitrogen (C-N) bonds. The peak at 500-700 cm-1 corresponds to the stretching vibration of the Zn-O bond, characteristic of zinc oxide [37]. ZnO NPs demonstrate a peak at 674 cm-1, confirming the presence of the Zn-O bond.

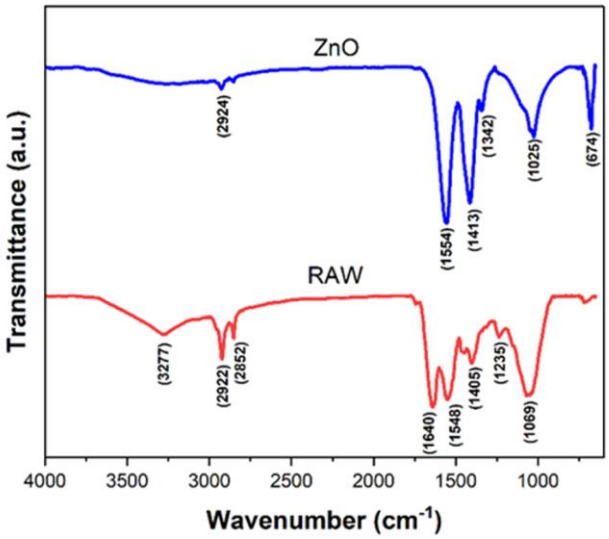

Figure 3. FTIR spectrum of raw cellar spider and synthesized ZnO NPs.

3.1.2 X-ray Diffraction Analysis (XRD)

The X-ray diffraction (XRD) pattern of ZnO nanoparticles exhibits peaks corresponding to crystal planes (100), (002), (101), (102), (110), (103), (200), and (112) [26]. These peaks, along with their relative intensities, provide insights into the crystal structure and orientation of the ZnO nanoparticles. Fig. 4 shows peaks (110), (112), (222), and (132) indicating the presence of ZnO crystal planes at (110) and (112), while the RAW (cellar spider) material exhibits peaks (104) and (113). The peak positions (2θ) are observed at values of 13.319, 33.077, 58.435, and 69.785, representing the angles of diffraction peaks. The intensity values associated with the peaks are 462, 1249, 665, and 320, with the second peak at 33.077 exhibiting the highest intensity. The estimated crystallite size values are 23.663 nm, 5.372 nm, 4.389 nm, and 7.943 nm, indicating the average size of crystalline domains within the material. Further quantitative analysis can be found in Table 1.

Table 1 Quantitative analysis on XRD data

Peak Position (2Θ)	Intensity	FWHM	Crystallite Size (nm)
13.319	462	0.345	23.663
33.077	1249	1.765	5.372
58.435	665	3.458	4.389
69.785	320	2.894	7.943
Average size (nm)		10.342	

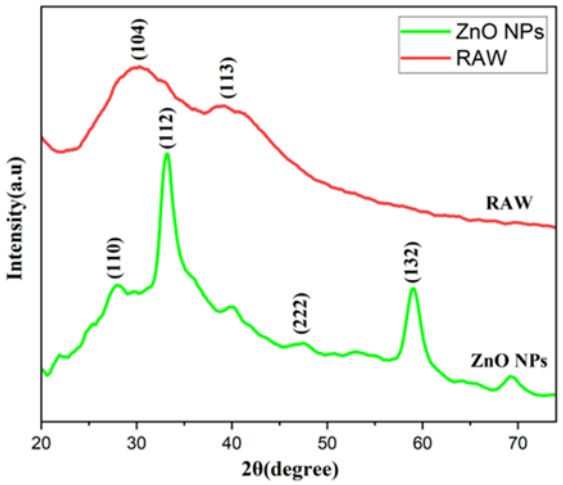

Figure 4. XRD diffraction peak of ZnO NPs and RAW.

3.1.3 Zeta Potential Characterization

In figure 5, Peak 1 exhibits the largest particles, with an average size of 584.1 nm, accounting for 81.0% of the volume. This peak demonstrates a varied population of larger particles, as evidenced by its high standard deviation of 99.32 nm. On the other hand, Peak 2 displays smaller particles, averaging 62.99 nm, comprising 19.0% of the volume. The decreased standard deviation of 8.010 nm suggests a more uniform distribution of tiny particles within this peak. The data depicts a bimodal distribution with two peaks representing different particle sizes. Peak 1 contains a greater number of particles compared to Peak 2. Both peaks exhibit a substantial volume, indicating a diverse range of particle sizes [38].

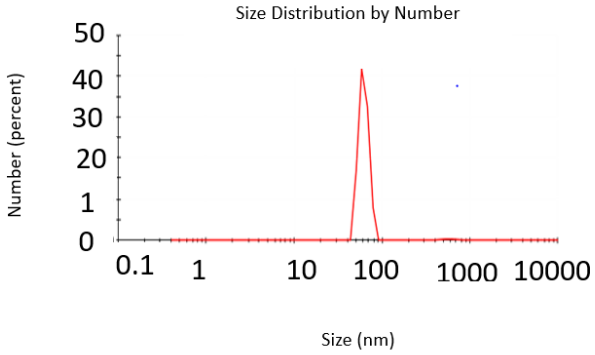

Figure 5. (A) zeta potential and (B) hydrodynamic size of ZnO NP.

3.2.4 Thermogravimetric Analysis (TGA)

Figure 6 illustrates the weight reduction of zinc oxide nanoparticles as the temperature increases, as observed through Thermogravimetric Analysis (TGA). The weight decreases from 97.99% at 40°C to 56.22% at 680°C, indicating the breakdown of nanoparticles due to the applied heat. The derivative weight (%/min) measurements exhibit an increase as the temperature rises, indicating a faster breakdown rate, ranging from 0.3412%/min at 40°C to 0.1019%/min at 680°C. Notably, two significant weight loss periods are observed. Between 120°C and 160°C, the weight drops significantly from 92.07% to 86.74%, suggesting the decomposition or release of volatile components from the nanoparticles. Another weight reduction occurs between 160°C and 180°C, with the weight decreasing from 86.74% to 81.87%, indicating further decomposition or changes. Furthermore, TGA experiments conducted using alternative methods reveal that zinc oxide nanoparticles experience a total weight loss of 6.10% around 492°C, attributed to the removal of moisture content. No significant decomposition is observed beyond this point up to 700°C [39]. The results from TGA investigations suggest that zinc oxide nanoparticles are thermally stable up to a certain temperature, with a gradual weight loss indicating a steady breakdown.

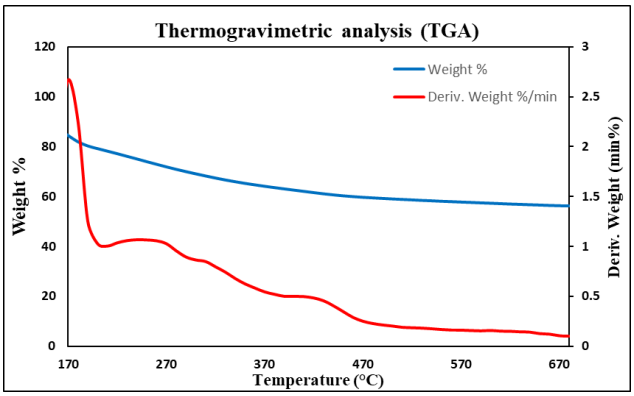

Figure 6. TGA result for ZnO nanoparticles.

3.2.5 UV-Visible Spectroscopy

In the UV-Vis spectrum, the signal amplitude around 360 nm was substantially reduced, indicating that the ion Zn cation may have been converted to metallic silver. This phenomenon was comparable to a previous study in which zinc oxide nanoparticles were synthesised using an artichoke leaf (Cynara scolymus) aqueous extract. Examining the UV-Vis spectrum, which is a common technique for characterizing zinc oxide nanoparticles [40], the researchers found an increase in absorbance in the range of 320-335 nm in that study (Figure 7).

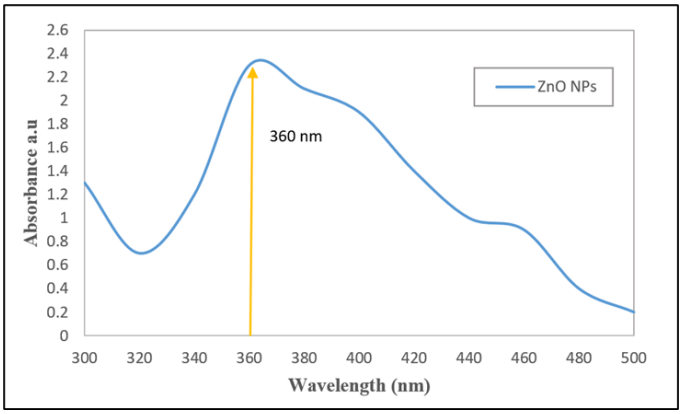

Figure 7. UV-Vis spectra of ZnO NPs.

3.2.6 Water Absorption Activity

Figure 8(a) shows the linear adsorption isotherm plots for MB adsorption on Zinc Oxide NPs for Langmuir and Freundlich models isotherm. According to the results, the Freundlich isotherm model had a better fit to the experimental data than Langmuir, considering its highest R^2 value (0.9824), indicating that the adsorption of MB onto Zinc Oxide NPs is a multiplayer process and that the adsorption capacity of the solid is not constant, but increases with increasing concentration of the solute in the solution. The Freundlich model is commonly used for adsorption of solutes onto heterogeneous adsorbents, where the adsorption sites on the solid surface have different affinities for the solute. It also a simple and widely used tool for describing adsorption behavior, but it is not always suitable for all types of adsorption processes and should be used with caution, taking into consideration the specific characteristics of the adsorption system [41].

As shown in Figure 8(b), the pseudo-second-order kinetic model had the highest R2 value (0.9997), indicating that it best describes the adsorption of MB onto Zinc Oxide NPs. Consequently, the pseudo-second-order model was found to best fit the experimental data, suggesting that the rate-controlling phase of adsorption is chemisorption involving valence forces through sharing and exchanging electrons between Zinc Oxide NPs and MB dye ions in solution [42]. Frequently, the pseudo-second-order model is applied to characterise the adsorption of solutes onto solid surfaces, such as in environmental remediation, effluent treatment, and drug delivery.

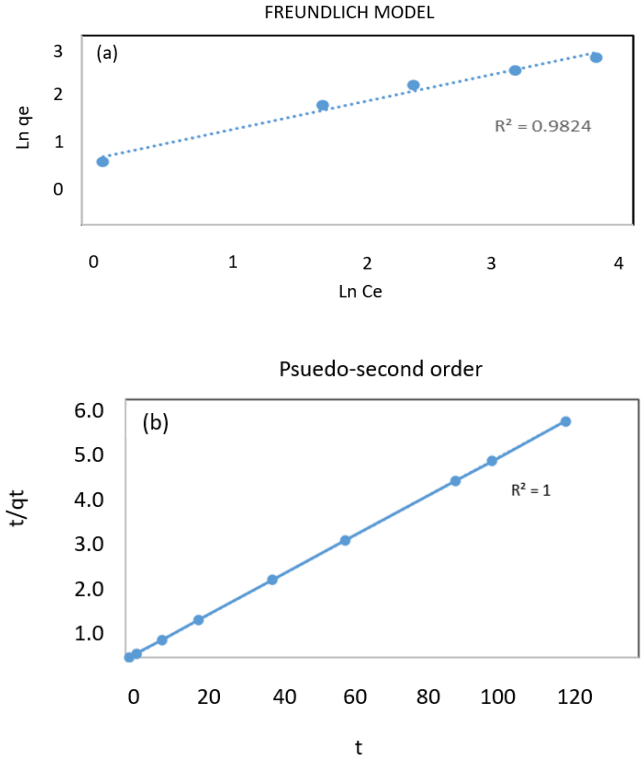

Figure 8. The linear adsorption plots for MB adsorption on Zinc Oxide NPs: (a)Freundlich isotherm and (b)Psuedo-second order.

The initial concentration of the pigment is another crucial factor influencing the adsorption procedure. Fig. 9 illustrates the MB removal efficiency and adsorption capacity of Zinc Oxide NPs at various initial MBTconcentrations. The MB removal efficacy decreased from 88.35% to 16.77% when the initial MB concentration was increased from 10 to 50 ppm, according to the results. In general, the quantity of accessible active sites at a fixed adsorbent dosage was increased to accommodate the low number of MB dye molecules in the solution when the initial MB concentration was low. However, when there were more MB dye molecules in the solution owing to a higher initial MB concentration, the available adsorption sites of Zinc Oxide NPs became saturated. Consequently, MB adsorption on Zinc Oxide NPs was prohibited. Next, a higher initial dye concentration provided a stronger driving force to surmount the mass transfer resistance of dye between the bulk liquid phase and solid phase, thereby increasing the adsorption capacity of the adsorbent. When the initial MB concentration increased from 10 to 50 ppm, the adsorption capacity of Zinc Oxide NPs increased from 8.83 mg/g to 21.89 mg/g. It is depicted in figure 9.

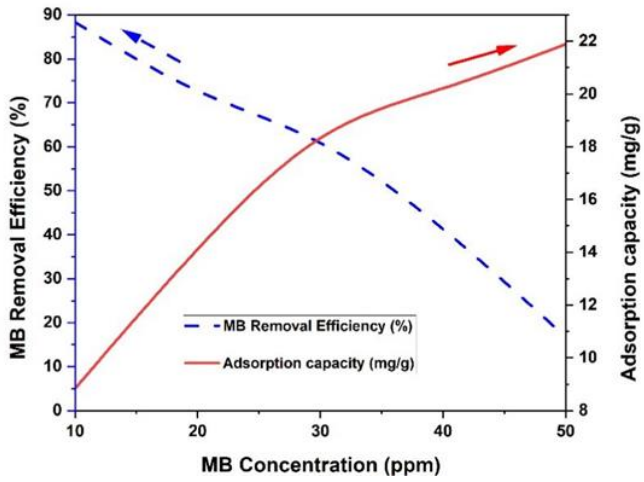

Figure 9. Influence of MB initial concentration on the MB removal efficiency and Zinc Oxide NPs adsorption capacity at the following condition: 20 mg of Zinc Oxide NPs; 20 mL of volume; and agitation time of 1 H.

CONCLUSION

In conclusion, the study explored the potential of utilizing cellar spider silk for the synthesis of silver nanoparticles. The FTIR spectra analysis revealed the presence of surface hydroxyl groups, C-H stretching vibrations, and carbon-nitrogen bonds in both raw cellar spider and synthesized ZnO NPs. X-ray Diffraction (XRD) analysis demonstrated distinctive peaks corresponding to ZnO crystal planes, providing insights into the crystal structure and orientation of the nanoparticles. Zeta potential characterization depicted a bimodal distribution of particles, indicating diverse sizes. Thermogravimetric Analysis (TGA) illustrated the thermal stability of ZnO nanoparticles up to a certain temperature, with gradual weight loss suggesting a steady breakdown. UV-Visible Spectroscopy indicated a potential conversion of Zn cation to metallic silver. The water absorption activity analysis

revealed the efficiency of ZnO NPs in adsorbing methylene blue (MB), with the Freundlich isotherm and pseudo-second-order kinetic model fitting the experimental data well. The study underscored the multifaceted characterization of ZnO NPs synthesized from cellar spider extracts, showcasing their potential in diverse applications, particularly in the field of nanotechnology and environmental remediation.

ACKNOWLEDGMENTS

We would like to express our gratitude to the Institute of Nanoelectronic Engineering (INEE) and the Faculty of Chemical Engineering Technology at the University of Malaysia Perlis, in addition to the technical workers, for making their facilities and help in this project available to us.

REFERENCES

[1] T. Balasubramaniam, A. H. A. Bakar, M. N. A. Uda, U. Hashim, N. A. Parmin, A. Anuar, M. A. A. Bakar, M. N. Afnan Uda, M. K. Sulaiman, Potential of Syntesized Silica Nanoparticles (Si-NPs) using Corn Cob for Arsenic Heavy Metal Removal, IOP Conf. Ser. Mater. Sci. Eng. 864 (2020) 0–5. https://doi.org/10.1088/1757-899X/864/1/012187.

[2] M. N. A. Uda, S. C. B. Gopinath, U. Hashim, M. N. Afnan Uda, N. A. Parmin, N. H. Halim, P. Anbu, Novelty Studies on Amorphous Silica Nanoparticle Production from Rice Straw Ash, IOP Conf. Ser. Mater. Sci. Eng. 864 (2020). https://doi.org/10.1088/1757-899X/864/1/012021.

[3] M. N. A. Uda, S. C. B. Gopinath, U. Hashim, M. N. Afnan Uda, N. H. Ibrahim, N. A. Parmin, N. H. Halim, P. Anbu, Simple and Green Approach Strategy to Synthesis Graphene Using Rice Straw Ash, IOP Conf. Ser. Mater. Sci. Eng. 864 (2020). https://doi.org/10.1088/1757-899X/864/1/012181.

[4] G. R. Uda MNA, Gopinath SCB, Hashim U, Uda MNA, Adam T, Parmin NA, Subramaniam S, Chinni SV, Lebaka VR, Controlling Arsenic Accumulation in Rice Grain under Nanomaterials-Assisted Optimal Greenhouse Set-Up, Sustainability. 15 (2023).

[5] M. N. A. Uda, C. M. Hasfalina, A. A. Samsuzanaa, S. Faridah, I. Zamri, B. S. Noraini, W. N. Sabrina, U. Hashim, S. C. B. Gopinath, Immunosensor development formatting for tungro disease detection using nano-gold antibody particles application, AIP Conf. Proc. 1808 (2017). https://doi.org/10.1063/1.4975290.

[6] A. H. M, M. N. A. Uda, S. C. B. Gopinath, Z. A. Arsat, F. Abdullah, M. F. A. Muttalib, M. K. R. Hashim, U. Hashim, M. N. A. Uda, A. R. W. Yaakub, N. H. Ibrahim, N. A. Parmin, T. Adam, Green route synthesis of antimicrobial nanoparticles using sewage alga bloom, Mater. Today Proc. (2023). https://doi.org/10.1016/j.matpr.2023.01.008.

[7] H. M. Azwatul, M. N. A. Uda, S. C. B. Gopinath, Z. A. Arsat, F. Abdullah, M. F. A. Muttalib, M. K. R. Hashim, U. Hashim, M. Isa, M. N. A. Uda, A. Radi Wan Yaakub, N. H. Ibrahim, N. A. Parmin, T. Adam, Plant-based green synthesis of silver nanoparticle via chemical bonding analysis, Mater. Today Proc. (2023). https://doi.org/10.1016/j.matpr.2023.01.005.

[8] H. M. Azwatul, M. N. A. Uda, S. C. B. Gopinath, Z. A. Arsat, F. Abdullah, M. F. A. Muttalib, M. K. R. Hashim, U. Hashim, M. Isa, M. N. A. Uda, A. Radi Wan Yaakub, N. H. Ibrahim, N. A. Parmin, T. Adam, Synthesis and characterization of silver nanoparticle using sewage algal bloom extract using visual parameter analysis, Mater. Today Proc. (2023). https://doi.org/10.1016/j.matpr.2023.01.004.

[9] R. Ghosh Chaudhuri, S. Paria, Core/shell nanoparticles: Classes, properties, synthesis mechanisms, characterization, and applications, Chem. Rev. 112 (2012) 2373–2433. https://doi.org/10.1021/cr100449n.

[10] P. Anbu, S. C. B. Gopinath, H. Shik, C. Lee, Temperature-dependent green biosynthesis and characterization of silver nanoparticles using balloon fl ower plants and their antibacterial potential, J. Mol. Struct. 1177 (2019) 302–309. https://doi.org/10.1016/j.molstruc.2018.09.075.

[11] T. Adam, U. Hashim, M. Mohan, M. N. A. Uda, M. N. A. Uda, Integrated ZnO-Al2O3 nano particles as absorbent for heavy metal ions and organic impurities, AIP Conf. Proc. 2339 (2021). https://doi.org/10.1063/5.0044235.

[12] G. Mehdi, Green synthesis, characterization and antimicrobial activity of silver nanoparticles (AgNPs) using leaves and stems extract of some plants, Adv. J. Chem. A. 2 (2019) 266–275. https://doi.org/10.33945/sami/ajca.2019.4.1.

[13] S. Gobalakrishnan, N. Chidhambaram, M. Chavali, Role of greener syntheses at the nanoscale, Handb. Greener Synth. Nanomater. Compd. Vol. 1 Fundam. Princ. Methods. (2021) 107–134. https://doi.org/10.1016/B978-0-12-821938-6.00004-9.

[14] A. Lateef, S. A. Ojo, M. A. Azeez, T. B. Asafa, T. A. Yekeen, A. Akinboro, I. C. Oladipo, E. B. Gueguim-Kana, L. S. Beukes, Cobweb as novel biomaterial for the green and eco-friendly synthesis of silver nanoparticles, Appl. Nanosci. 6 (2016) 863–874. https://doi.org/10.1007/s13204-015-0492-9.

[15] A. Sirelkhatim, S. Mahmud, A. Seeni, N. H. M. Kaus, L. C. Ann, S. K. M. Bakhori, H. Hasan, D. Mohamad, Review on zinc oxide nanoparticles: Antibacterial activity and toxicity mechanism, Nano-Micro Lett. 7 (2015) 219–242. https://doi.org/10.1007/s40820-015-0040-x.

[16] T. U. Doan Thi, T. T. Nguyen, Y. D. Thi, K. H. Ta Thi, B. T. Phan, K. N. Pham, Green synthesis of ZnO nanoparticles using orange fruit peel extract for antibacterial activities, RSC Adv. 10 (2020) 23899–23907. https://doi.org/10.1039/d0ra04926c.

[17] Y. Wang, W. Shi, T. Wen, Prediction of winter wheat yield and dry matter in North China Plain using machine learning algorithms for optimal water and nitrogen application, Agric. Water Manag. 277 (2023) 108140. https://doi.org/10.1016/j.agwat.2023.108140.

[18] A. C. Burdușel, O. Gherasim, A. M. Grumezescu, L. Mogoantă, A. Ficai, E. Andronescu, Biomedical applications of silver nanoparticles: An up-to-date overview, Nanomaterials. 8 (2018) 1–25. https://doi.org/10.3390/nano8090681.

[19] J. Vega-Baudrit, S. M. Gamboa, E. R. Rojas, V. V. Martinez, Synthesis and characterization of silver nanoparticles and their application as an antibacterial agent, Int. J. Biosens. Bioelectron. 5 (2019). https://doi.org/10.15406/ijbsbe.2019.05.00172.

[20] D. Jain, Shivani, A. A. Bhojiya, H. Singh, H. K. Daima, M. Singh, S. R. Mohanty, B. J. Stephen, A. Singh, Microbial Fabrication of Zinc Oxide Nanoparticles and Evaluation of Their Antimicrobial and Photocatalytic Properties, Front. Chem. 8 (2020) 1–11. https://doi.org/10.3389/fchem.2020.00778.

[21] M. N. A. Uda, S. C. B. Gopinath, U. Hashim, N. H. Halim, N. A. Parmin, M. N. Afnan Uda, A. Tijjani, A. Periasamy, Silica and graphene mediate arsenic detection in mature rice grain by a newly patterned current – volt aptasensor, Sci. Rep. 11 (2021) 1–13. https://doi.org/10.1038/s41598-021-94145-0.

[22] M. N. Afnan Uda, A. B. Jambek, U. Hashim, M. N. A. Uda, Electrical DNA Biosensor Using Aluminium Interdigitated Electrode for Salmonella Detection, IOP Conf. Ser. Mater. Sci. Eng. 743 (2020). https://doi.org/10.1088/1757-899X/743/1/012022.

[23] M. N. A. Uda, T. Adam, U. Hashim, A. B. Mosbah, M. N. A. Uda, MPTES decorated IDE for arsenic (AS) selective detection, AIP Conf. Proc. 2339 (2021). https://doi.org/10.1063/5.0044562.

[24] U. Hashim, T. Adam, N. A. K. H. Ehfaed, M. N. A. Uda, M. N. A. Uda, Quantitative lead (Pb+) ion detection via modified silicon nanowire, AIP Conf. Proc. 2339 (2021). https://doi.org/10.1063/5.0044568.

[25] L. Azeez, A. Lateef, S. A. Adebisi, A. O. Oyedeji, Novel biosynthesized silver nanoparticles from cobweb as adsorbent for Rhodamine B: equilibrium isotherm, kinetic and thermodynamic studies, Appl. Water Sci. 8 (2018) 1–12. https://doi.org/10.1007/s13201-018-0676-z.

[26] M. Naseer, U. Aslam, B. Khalid, B. Chen, Green route to synthesize Zinc Oxide Nanoparticles using leaf extracts of Cassia fistula and Melia azadarach and their antibacterial potential, Sci. Rep. 10 (2020) 1–10. https://doi.org/10.1038/s41598-020-65949-3.

[27] T. Fiore, C. Pellerito, Infrared Absorption Spectroscopy, Spectrosc. Mater. Charact. (2021) 129–167. https://doi.org/10.1002/9781119698029.ch5.

[28] M. N. A. Uda, S. C. B. Gopinath, U. Hashim, N. H. Halim, N. A. Parmin, M. N. Afnan Uda, P. Anbu, Production and characterization of silica nanoparticles from fly ash: conversion of agro-waste into resource, Prep. Biochem. Biotechnol. 51 (2021) 86–95. https://doi.org/10.1080/10826068.2020.1793174.

[29] A. Kumar, C. K. Dixit, Methods for characterization of nanoparticles, Adv. Nanomedicine Deliv. Ther. Nucleic Acids. (2017) 44–58. https://doi.org/10.1016/B978-0-08-100557-6.00003-1.

[30] N. H. Daraghmeh, B. Z. Chowdhry, S. A. Leharne, M. M. Al Omari, A. A. Badwan, Chitin, 1st ed., Elsevier Inc., 2011. https://doi.org/10.1016/B978-0-12-387667-6.00002-6.

[31] J. Kalmár, G. Lente, I. Fábián, Kinetics and mechanism of the adsorption of methylene blue from aqueous solution on the surface of a quartz cuvette by on-line UV-Vis spectrophotometry, Dye. Pigment. 127 (2016) 170–178. https://doi.org/10.1016/j.dyepig.2015.12.025.

[32] Sachin, Jaishree, N. Singh, R. Singh, K. Shah, B. K. Pramanik, Green synthesis of zinc oxide nanoparticles using lychee peel and its application in anti-bacterial properties and CR dye removal from wastewater, Chemosphere. 327 (2023) 138497. https://doi.org/10.1016/j.chemosphere.2023.138497.

[33] K. Handore, S. Bhavsar, A. Horne, P. Chhattise, K. Mohite, J. Ambekar, N. Pande, V. Chabukswar, Novel green route of synthesis of ZnO nanoparticles by using natural biodegradable polymer and its application as a catalyst for oxidation of aldehydes, J. Macromol. Sci. Part A Pure Appl. Chem. 51 (2014) 941–947. https://doi.org/10.1080/10601325.2014.967078.

[34] N. N. Rupiasih, W. G. Suharta, M. Sumadiyasa, M. N. Islami, The Current-Voltage Properties of Ch/AgNP Composite Membranes: A Study on the Effect of AgNP Content, IOP Conf. Ser. Mater. Sci. Eng. 515 (2019). https://doi.org/10.1088/1757-899X/515/1/012064.

[35] A. Barth, Infrared spectroscopy of proteins, Biochim. Biophys. Acta - Bioenerg. 1767 (2007) 1073–1101. https://doi.org/10.1016/j.bbabio.2007.06.004.

[36] P. J. Larkin, General Outline for IR and Raman Spectral Interpretation, Infrared Raman Spectrosc. (2018) 135–151. https://doi.org/10.1016/b978-0-12-804162-8.00007-0.

[37] G. Nagaraju, Udayabhanu, Shivaraj, S. A. Prashanth, M. Shastri, K. V. Yathish, C. Anupama, D. Rangappa, Electrochemical heavy metal detection, photocatalytic, photoluminescence, biodiesel production and antibacterial activities of Ag–ZnO nanomaterial, Mater. Res. Bull. 94 (2017) 54–63. https://doi.org/10.1016/j.materresbull.2017.05.043.

[38] K. M. Kim, T. H. Kim, H. M. Kim, H. J. Kim, G. H. Gwak, S. M. Paek, J. M. Oh, Colloidal behaviors of ZnO nanoparticles in various aqueous media, Toxicol. Environ. Health Sci. 4 (2012) 121–131. https://doi.org/10.1007/s13530-012-0126-5.

[39] T. W. Quadri, L. O. Olasunkanmi, O. E. Fayemi, M. M. Solomon, E. E. Ebenso, Zinc Oxide Nanocomposites of Selected Polymers: Synthesis, Characterization, and Corrosion Inhibition Studies on Mild Steel in HCl Solution, ACS Omega. 2 (2017) 8421–8437. https://doi.org/10.1021/acsomega.7b01385.

[40] K. P. Bhandari, D. R. Sapkota, M. K. Jamarkattel, Q. Stillion, R. W. Collins, Zinc Oxide Nanoparticles — Solution-Based Synthesis and Characterizations, (2023) 1–15.

[41] M. A. Al-Ghouti, D. A. Da'ana, Guidelines for the use and interpretation of adsorption isotherm models: A review, J. Hazard. Mater. 393 (2020) 122383. https://doi.org/10.1016/j.jhazmat.2020.122383.

[42] J. C. Bullen, S. Saleesongsom, K. Gallagher, D. J. Weiss, A Revised Pseudo-Second-Order Kinetic Model for Adsorption, Sensitive to Changes in Adsorbate and Adsorbent Concentrations, Langmuir. 37 (2021) 3189–3201. https://doi.org/10.1021/acs.langmuir.1c00142.